

Reference Deconvolution: A Simple and Effective Method for Resolution Enhancement in Nuclear Magnetic Resonance Spectroscopy

K. R. METZ,¹ M. M. LAM,² A. G. WEBB²

¹Department of Radiology, New England Deaconess Hospital, Harvard Medical School, Boston, MA 02215

²Department of Electrical and Computer Engineering, University of Illinois at Urbana-Champaign, 1406 West Green Street, Urbana, IL 61801

ABSTRACT: Linewidths and line shapes are key criteria determining the utility of a nuclear magnetic resonance (NMR) spectrum, and considerable effort is usually devoted to shimming the magnetic field (B_0) to ensure optimum resolution. However, even if the external field is almost perfectly homogeneous, the sample itself can induce gradients owing to susceptibility effects from its overall shape or internal heterogeneity. Thus, magnetic field gradients nearly always contribute significantly to the linewidths and shapes in an NMR spectrum. Reference deconvolution is a technique which uses the shape of a single resonance line to measure the actual frequency distribution produced by the local B_0 inhomogeneity and then deconvolves that distribution from the whole spectrum. It is a simple linear process which requires no prior knowledge of the number of lines, their intensities, or their relaxation characteristics. No fitting procedures are used. This article reviews the reference deconvolution method, demonstrates its application to one-dimensional NMR spectroscopy, and discusses the tradeoffs between resolution and signal / noise. © 2000 John Wiley & Sons, Inc. Concepts Magn Reson 12: 21–42, 2000

KEY WORDS: reference deconvolution; magnetic field inhomogeneities; NMR line shape distortions; spectral resolution; signal / noise

Received 14 May 1999; revised 25 August 1999;
accepted 26 August 1999.

Correspondence to: A. G. Webb; E-mail: a-webb2@uiuc.edu.

Concepts in Magnetic Resonance, Vol. 12(1) 21–42 (2000)

© 2000 John Wiley & Sons, Inc. CCC 1043-7347/00/010021-22

INTRODUCTION

High-resolution nuclear magnetic resonance (NMR) spectroscopy is one of the most widely used analytical techniques for structure determination. Chemical species which are amenable to study range from simple ions to complex biomacromolecules with molecular weights of 40 kD or higher. NMR is also able to characterize weak interactions between macromolecules and ligands, information which is particularly important in the pharmaceutical industry. With recent advances in hardware and software, total sample quantities of < 1 nmol can now be studied. In high-resolution NMR, the information that enables structural analyses to be performed includes signal intensities, chemical shifts, scalar couplings, through-space couplings, and relaxation times. High spectral resolution is important for the measurement of each of these parameters, especially for signal intensities, chemical shifts, and coupling constants. Any distortions in the magnetic field (B_0) over the sample volume cause line broadening, which makes such measurements more difficult if not impossible. As an indication, typical proton scalar coupling constants lie in the range of 4–7 Hz. At an operating frequency of 500 MHz (14.1 Tesla), a linewidth of 5 Hz, which would obscure these couplings, corresponds to a magnetic field variation of only 1 part in 10^8 over the sample. It is clear, then, that very small imperfections in field homogeneity can have drastic implications for spectral quality. Considerable effort is usually expended in maximizing the resolution, including careful shimming, sample spinning, the rigorous exclusion of paramagnetic or particulate impurities from the sample, and the use of magnetic susceptibility matched glasses for sample containment. Further details on techniques for the optimization of B_0 homogeneity can be found in earlier articles published in this journal (1–3).

In a number of situations outlined later in this article, the best achievable magnetic field homogeneity is still relatively poor and yields insufficient spectral resolution for accurate determination of chemical shifts or scalar coupling constants. To perform these measurements, it is often possible to improve the resolution by some form of postprocessing. Reference deconvolution is a simple and robust resolution enhancement technique that has been applied by a number of investigators to high-resolution NMR studies (4–16). In its simplest form, it efficiently removes

line shape distortions from the spectrum, so that the final shapes are purely Lorentzian and the widths are limited only by the spin–spin relaxation time (T_2) of each resonance.

SOURCES OF B_0 INHOMOGENEITY

Before considering the technical details of reference deconvolution, we first summarize possible sources of magnetic field distortion to highlight cases in which the technique finds particular application. For more thorough discussions, Refs. 1–3 and 17–19 are particularly useful.

Imperfect Shim

Magnetic field shimming is a routine part of almost every high-resolution NMR measurement. The reason for this is obvious: badly shimmed samples produce poorly resolved spectra with inferior signal/noise (S/N). Despite its importance, however, exhaustive shimming may not be practical or productive in all situations. For example, if the experiment is intended to monitor an ongoing chemical reaction, only a short time may be available for shimming before spectra must be acquired. Another example is *in vivo* NMR, in which physiological constraints may prevent animals from being anesthetized or otherwise immobilized for long periods. Even for conventional, stable samples, small external field inhomogeneities will inevitably remain even after the most aggressive shimming.

Small Sample Size

For a mass-limited sample, optimum sensitivity is usually achieved by studying a concentrated solution which has been confined to the smallest practical volume (20). However, unless the sample is a sphere or an infinitely long cylinder, magnetic susceptibility discontinuities present at its surface will produce local inhomogeneities in the magnetic field, causing NMR line shape distortions which cannot be shimmed. To help minimize this problem, so-called susceptibility plugs are increasingly being used to confine samples to small regions of standard NMR tubes. The bulk magnetic susceptibility of the plug is chosen to match that of the sample as closely as practical, thus minimizing discontinuities at the plug/sample interface. The problem is that the match is never perfect, so susceptibility variations still ex-

ist, and to make matters worse, they occur close to or even inside the most sensitive region of the radiofrequency (rf) probe.

Proximity of the Sample and rf Coil

For optimum spectral sensitivity, the rf coil should be located as close to the sample as possible (20). Either copper or silver is normally used as the conductor since they have the lowest resistance of all the common metals. This results in minimum noise from the coil. Unfortunately, these metals are also paramagnetic ($\chi_v = -1.892 \times 10^{-6}$ cgs for silver and -0.768×10^{-6} cgs for copper) and produce considerable distortion of the local magnetic field. The most direct solution to this problem is to use zero-susceptibility wire, which can be rhodium-plated copper (21) or aluminum-clad copper (17, 19). Although they reduce the mismatch, often these materials are only zero susceptibility to within 5%, and for small probes with high filling factors, they can still produce considerable distortions in line shape.

Nonspinning Samples

After all reasonable efforts have been made to minimize magnetic field variations in the sample, further improvements in spectral line shapes and widths can be achieved by spinning the sample, a process which averages radial field inhomogeneities and reduces their line-broadening effects (22). Sample spinning typically improves the resolution by a factor of 3–10. Therefore, if the sample cannot be spun, the linewidths and shapes will often be dominated by the effects of local magnetic field inhomogeneity rather than the natural T_2 . Some types of NMR experiments are usually performed without sample spinning, including spin-echo-based sequences, where spinning can cause a time-dependent modulation of the NMR signal that interferes with data analysis. Also, a growing trend has been the application of NMR to large, bulky samples which are unsuited to spinning. An obvious example would be *in vivo* specimens, especially whole animals and perfused organs.

Samples with Intrinsic Spatial Inhomogeneity

Unlike the pure uniform liquids used for high-resolution NMR, some samples are by nature magnetically and spatially heterogeneous. Exam-

ples would include coarse polymer blends, unrefined geological materials such as coal and oil well cores, and most *in vivo* samples. Biological tissues are inherently complex (Fig. 1) and contain many sources of local field inhomogeneities (23). For instance, in the brain there are magnetic susceptibility differences between white and gray matter, resulting in field discontinuities at the interfaces between these different tissue types. Other interfaces exist between the bulk tissue and bone (24) or air-filled sinuses (25). Blood inside the capillaries contains several paramagnetic compounds such as hemoglobin which cause magnetic susceptibility gradients across the tissue (26). Some biological tissues also have ferromagnetic iron deposits that can exert powerful local effects on field homogeneity. For simple *in vivo* studies on muscle, the interfaces and geometries of different muscle fibers give rise to considerable magnetic field inhomogeneities. Even macroscopically uniform tissues like liver are densely packed with blood vessels and bile ducts having different susceptibilities from the surrounding cells. Finally, the cells themselves contain a multitude of organelles, cytoskeletal fibers, and a matrix of internal membranes, all producing magnetic microheterogeneities in the surrounding intracellular fluids from which the NMR signals arise. The net result of all this structural complexity is that *in vivo* linewidths are nearly always dominated

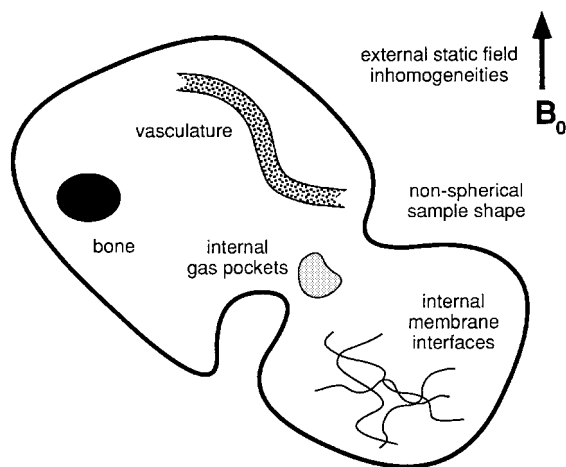


Figure 1 Sources of local magnetic field inhomogeneity for *in vivo* samples. Susceptibility discontinuities occur at every interface between regions of differing chemical composition (i.e., water/lipid membrane, water/bone, water/air). Also, unless the sample is spherical, its overall shape produces magnetic field gradients even if the applied, external field is perfectly homogeneous.

by magnetic field inhomogeneities, and widths of <0.1 ppm are practically impossible to achieve for many tissues.

NMR LINE SHAPES

For a single type of spin in a perfectly homogeneous B_0 field, the ideal time-domain NMR signal is usually given by a complex, exponentially damped sinusoid:

$$s_{\text{homog}}(t) = M_0 \cdot [\cos(2\pi\nu t) - i \cdot \sin(2\pi\nu t)] \cdot e^{-t/T_2} \quad [1]$$

where M_0 is the initial amplitude at time 0 and ν is the resonance frequency in Hertz. The damping constant T_2 depends intrinsically on the dynamic properties of the system. For example, in large proteins, T_2 is approximately inversely proportional to the overall rotational correlation time of the molecule and therefore depends on the protein's molecular weight, shape, and aggregation state, as well as the solvent viscosity and sample temperature. The frequency-domain NMR signal is computed by a complex Fourier transformation of the time-domain free induction decay (FID), with the real component usually being the signal displayed. The line shape is Lorentzian, and its width in Hertz is defined by a parameter termed the full width at half maximum (FWHM), shown in Figure 2. This is related to the exponential

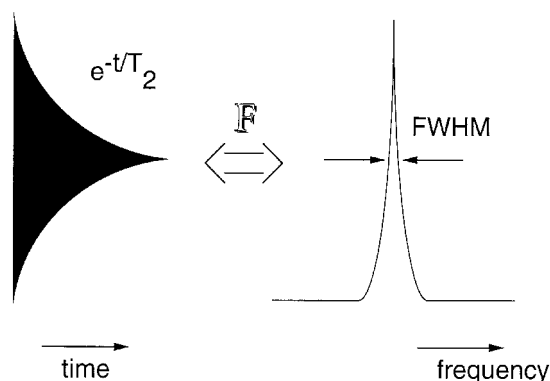


Figure 2 Time- and frequency-domain NMR signals in a perfectly homogeneous magnetic field. The time-domain free induction decay (FID) shown on the left corresponds to an exponentially damped sinusoid. The real part of the frequency-domain spectrum (right), obtained by Fourier transformation of the time-domain signal, has a Lorentzian shape with a width defined by the full width at half maximum amplitude (FWHM).

damping constant by:

$$\text{FWHM} = \frac{1}{\pi T_2} \quad [2]$$

In practice, a perfectly homogeneous magnetic field can never be produced, and the distribution of fields ΔB_0 present in the sample causes the spins to resonate over a range of different frequencies $\Delta\nu_0$:

$$\Delta\nu_0 = \frac{\gamma}{2\pi} \cdot \Delta B_0 \quad [3]$$

where γ is the magnetogyric ratio in $\text{rad s}^{-1} \text{T}^{-1}$. Destructive interference among the resulting sinusoids makes the time-domain signal decay more rapidly. Assuming the decay remains exponential, the damping constant in an inhomogeneous field is given the symbol T_2^* . This in turn can be decomposed into two terms: T_2 and T_2^+ , where T_2^+ represents contributions arising solely from inhomogeneities in the local magnetic field. By invoking Eqs. [2] and [3], the damping constant may be expressed as:

$$\frac{1}{T_2^*} = \frac{1}{T_2} + \frac{1}{T_2^+} = \frac{1}{T_2} + \frac{\gamma \cdot \Delta B_0}{2} \quad [4]$$

Thus, magnetic field inhomogeneities can cause the signal to decay exponentially but at a faster rate:

$$s_{\text{inhomog}}(t) = M_0 \cdot [\cos(2\pi\nu t) - i \cdot \sin(2\pi\nu t)] \cdot e^{-t/T_2} \cdot e^{-t/T_2^+} \quad [5]$$

which leads to an artificially broadened, though still Lorentzian frequency-domain line. Such broadening makes spectral overlap more likely, so signal integration, chemical shift assignments, and scalar coupling constant measurements are more difficult.

It is possible to change the linewidth artificially during postprocessing by multiplying the FID by an exponential function:

$$s_{\text{processed}}(t) = M_0 \cdot [\cos(2\pi\nu t) - i \cdot \sin(2\pi\nu t)] \cdot e^{-t/T_2} \cdot e^{-t/T_2^+} \cdot e^{-\pi W t} \quad [6]$$

The variable W has units of Hertz and is usually known as the line broadening parameter because using positive values causes the time-domain data to decay more quickly leading to an increased

linewidth in the frequency domain. However, if a negative value is chosen for W , line narrowing results (27, 28). In fact, using $W = -(\pi T_2^+)^{-1}$ exactly compensates for the effects of field inhomogeneity and recovers the original natural linewidth. Although this exponential multiplication technique produces resolution enhancement, it can severely degrade the S/N because it increases the amplitude of the tail of the FID where noise typically dominates.

Magnetic field inhomogeneities usually cause the FID to decay nonexponentially (Fig. 3), leading to non-Lorentzian line shapes in the frequency domain. Signal overlap in this case can seriously hinder spectral interpretation. The lines can still be narrowed by exponential multiplication, but since the time-domain decay is not a simple exponential, it is no longer possible to compensate exactly for field inhomogeneity effects using this method.

From a phenomenological point of view, an experimental NMR signal can be considered as a combination of several distinct frequency-domain components or their time-domain counterparts (Fig. 4). The resonance frequency is represented by a delta function, and this is mathematically convolved with an ideal, natural linewidth and shape $S_{ideal}(f)$. The resulting line is again convolved with an arbitrary instrumental line-broad-

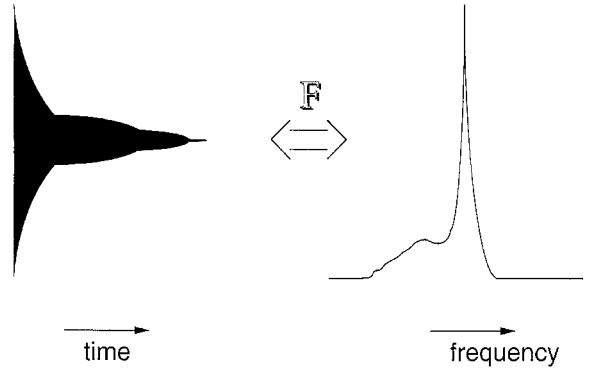


Figure 3 Time- and frequency-domain NMR signals in an inhomogeneous magnetic field. The time-domain FID (left) does not decay smoothly because the damping function is not a simple exponential. The real part of the corresponding frequency-domain spectrum (right) exhibits a non-Lorentzian line shape.

ening function $G(f)$, which in most cases has the shape of a histogram mapping the distribution of magnetic fields over the sample. Finally, noise in the frequency domain is added to the three convolved peak components to produce the final experimental peak. As shown in Figure 4, the experimental line shape may be dominated by instrumental contributions $G(f)$ instead of the natural shape and width $S_{ideal}(f)$. Since the field

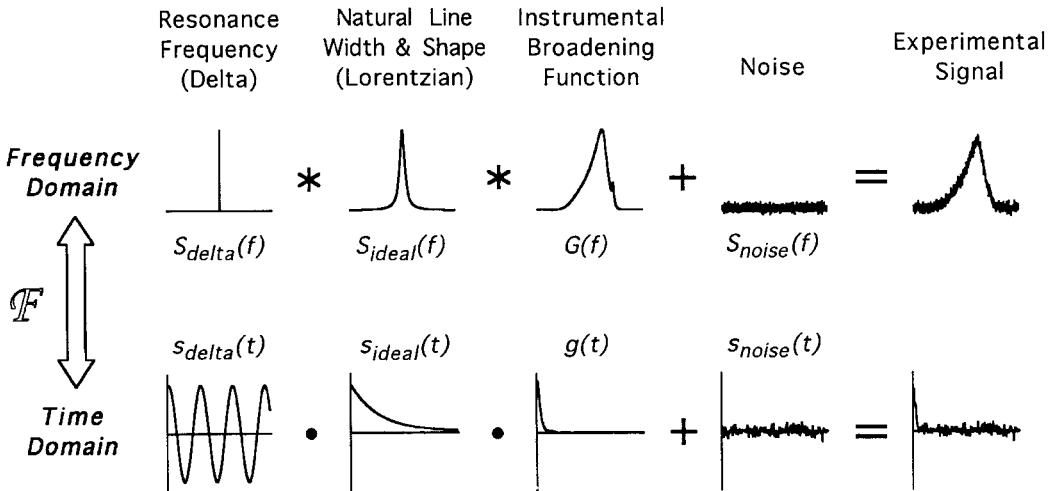


Figure 4 Components of an NMR signal. The time-domain (bottom) and frequency-domain (top) signals are related by the Fourier transform (left). Only the real parts in each domain are shown. $*$ = convolution; \cdot = multiplication. The frequency-domain peak is formed by convolving a delta function $S_{delta}(f)$, an ideal line shape and width $S_{ideal}(f)$, and an instrumental broadening function $G(f)$ determined mainly by the distribution of magnetic fields in the sample. The addition of frequency-domain noise produces the final experimental NMR peak. Corresponding signals in the time domain are combined by multiplication and addition.

homogeneity changes for each sample and shim settings, $G(f)$ also varies from one sample to the next.

$G(f)$ plays a central role in reference deconvolution. For spatially uniform samples, every peak in the NMR spectrum is distorted equally by this function (except for signals arising from zero- and multiple-quantum transitions). Therefore, if a single, well-resolved peak (termed the reference line) is present, its shape also contains $G(f)$. The reference deconvolution technique works by deconvolving the reference line from the “spectrum of interest,” thus eliminating $G(f)$ from all peaks and leaving signals composed only of delta functions, ideal line shapes, and noise.

MATHEMATICAL FRAMEWORK FOR REFERENCE DECONVOLUTION

We begin by assuming the existence of an ideal reference function $S_{\text{ideal}}(f)$, which represents a single peak with a linewidth w and a shape undistorted by magnetic field inhomogeneity or other instrumental effects. Under nonideal experimental conditions, $S_{\text{ideal}}(f)$ is the input to a linear frequency-invariant system $G(f)$ whose output is the experimental reference spectrum $S_{\text{ref}}(f)$. Noting that convolution in the frequency domain is the Fourier equivalent of multiplication in the time domain (Fig. 4), the results for nonideal conditions are:

$$S_{\text{ref}}(f) = S_{\text{ideal}}(f) * G(f) \quad [7a]$$

$$s_{\text{ref}}(t) = s_{\text{ideal}}(t) \cdot g(t) \quad [7b]$$

where $*$ represents convolution and \cdot represents multiplication. Next, we define an ideal spectrum of interest $S_{\text{comp}}(f)$ containing an arbitrary number of lines having widths and shapes undistorted by field inhomogeneity. Applying $G(f)$ to data set $S_{\text{comp}}(f)$ results in the experimentally observed spectrum $S_{\text{exp}}(f)$. The same system $G(f)$ in Eq. [7a] is used here since reference deconvolution assumes frequency independence. The input $S_{\text{comp}}(f)$ and output $S_{\text{exp}}(f)$ are related by:

$$S_{\text{exp}}(f) = S_{\text{comp}}(f) * G(f) \quad [8a]$$

$$s_{\text{exp}}(t) = s_{\text{comp}}(t) \cdot g(t) \quad [8b]$$

Rearranging Eq. [7b] as $g(t) = s_{\text{ref}}(t)/s_{\text{ideal}}(t)$ and substituting $g(t)$ into Eq. [8b], the signal $s_{\text{comp}}(t)$

and its Fourier transform are determined to be:

$$s_{\text{comp}}(t) = \frac{s_{\text{exp}}(t)}{g(t)} = \frac{s_{\text{exp}}(t) \cdot s_{\text{ideal}}(t)}{s_{\text{ref}}(t)} \quad [9]$$

$$S_{\text{comp}}(f) = FT \left\{ \frac{s_{\text{exp}}(t) \cdot s_{\text{ideal}}(t)}{s_{\text{ref}}(t)} \right\} \quad [10]$$

where FT is a forward Fourier transform. The result from Eq. [10] represents a compensated spectrum having ideal line shapes produced through the deconvolution process. Reference deconvolution can be interpreted as an amplitude and phase correction for each point of the FID and is equivalent to a deconvolution in the frequency domain. The net effect is to use $S_{\text{ideal}}(f)$, an ideal line shape and width, to correct for $G(f)$, the instrumental contribution to the line shapes and widths in the spectrum of interest.

PRACTICAL APPLICATION IN NMR SPECTROSCOPY

Figure 5 illustrates reference deconvolution processing steps for a case in which the reference line is part of the spectrum of interest. First, the experimental free induction decay $s_{\text{exp}}(t)$ is acquired [Fig. 5(A)]. Fourier transformation of $s_{\text{exp}}(t)$, followed by phasing and, if necessary, baseline correction produces the experimental spectrum $S_{\text{exp}}(f)$ shown in Fig. 5(B). The reference spectrum $S_{\text{ref}}(f)$ in Fig. 5(C) is obtained by windowing the experimental spectrum $S_{\text{exp}}(f)$ to suppress all components except the reference peak. Inverse Fourier transformation of $S_{\text{ref}}(f)$ then produces the time-domain reference signal $s_{\text{ref}}(t)$ [Fig. 5(D)]. Next, the reference peak from $S_{\text{ref}}(f)$ is replaced by a delta function $S_{\text{delta}}(f)$ at the frequency where $S_{\text{ref}}(f)$ has maximum amplitude. $S_{\text{delta}}(f)$ is subjected to inverse Fourier transformation, and the resulting time-domain signal $s_{\text{delta}}(t)$ is multiplied by $e^{-\pi w t}$ to produce $s_{\text{ideal}}(t)$, as shown in Fig. 5(E). The parameter w used for the exponential multiplication is termed the target linewidth. Fourier transformation of $s_{\text{ideal}}(t)$ produces the ideal Lorentzian peak $S_{\text{ideal}}(f)$ with FWHM = w [Fig. 5(F)]. Finally, Eqs. [9] and [10] are used to compute the final compensated time-domain signal $s_{\text{comp}}(t)$ and its spectrum $S_{\text{comp}}(f)$ displayed in Figs. 5(G) and 5(H), respectively.

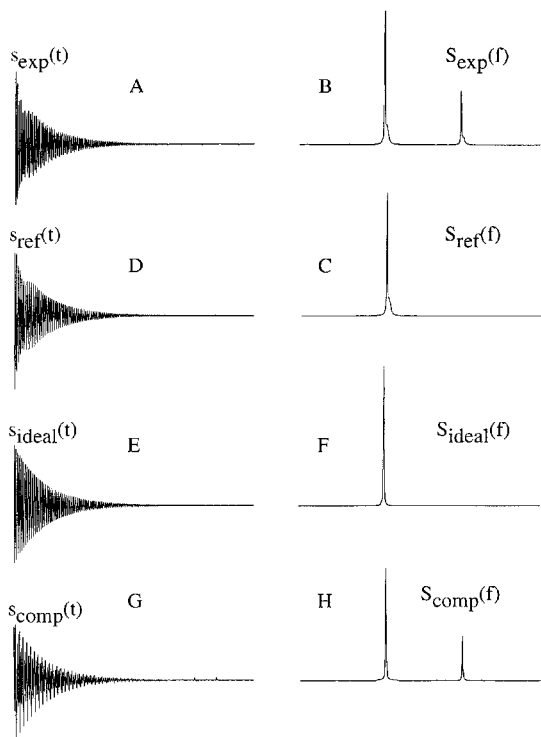


Figure 5 Steps in the reference deconvolution procedure. (A) Experimental FID $s_{\text{exp}}(t)$ is the acquired data. (B) Experimental spectrum $S_{\text{exp}}(f)$ is obtained by FT of $s_{\text{exp}}(t)$. (C) Reference spectrum $S_{\text{ref}}(f)$ is formed by windowing $S_{\text{exp}}(f)$ to remove all components except the reference line. (D) Reference FID $s_{\text{ref}}(t)$ is the inverse FT of $S_{\text{ref}}(f)$. (E) Ideal reference FID $s_{\text{ideal}}(t)$ is derived from a delta function $S_{\text{delta}}(f)$ located at the maximum of $S_{\text{ref}}(f)$ and modified by exponential multiplication. (F) Ideal reference spectrum $S_{\text{ideal}}(f)$ is the FT of $s_{\text{ideal}}(t)$. (G) Final compensated FID $s_{\text{comp}}(t)$ computed from Eq. [9]. (H) Final compensated spectrum $S_{\text{comp}}(f)$ computed by Fourier transformation of $s_{\text{comp}}(t)$ using Eq. [10].

It should be noted that Eqs. [9] and [10] employ complex multiplication and division, which are standard functions in many software packages. However, these operations can also be performed point by point by dividing $s_{\text{exp}}(t)$ by $s_{\text{ref}}(t)$ and then multiplying the quotient by $s_{\text{ideal}}(t)$:

$$\begin{aligned} \text{Re}_{\text{quot}}(t) &= \text{Re} \left\{ \frac{s_{\text{exp}}(t)}{s_{\text{ref}}(t)} \right\} \\ &= \frac{[\text{Re}_{\text{exp}} \cdot \text{Re}_{\text{ref}}] + [\text{Im}_{\text{exp}} \cdot \text{Im}_{\text{ref}}]}{[\text{Re}_{\text{ref}}]^2 + [\text{Im}_{\text{ref}}]^2} \end{aligned} \quad [11a]$$

$$\begin{aligned} \text{Im}_{\text{quot}}(t) &= \text{Im} \left\{ \frac{s_{\text{exp}}(t)}{s_{\text{ref}}(t)} \right\} \\ &= \frac{[\text{Im}_{\text{exp}} \cdot \text{Re}_{\text{ref}}] - [\text{Re}_{\text{exp}} \cdot \text{Im}_{\text{ref}}]}{[\text{Re}_{\text{ref}}]^2 + [\text{Im}_{\text{ref}}]^2} \end{aligned} \quad [11b]$$

$$\begin{aligned} \text{Re}\{s_{\text{comp}}(t)\} &= \text{Re}\{s_{\text{quot}}(t) \cdot s_{\text{ideal}}(t)\} \\ &= [\text{Re}_{\text{quot}} \cdot \text{Re}_{\text{ideal}}] - [\text{Im}_{\text{quot}} \cdot \text{Im}_{\text{ideal}}] \end{aligned} \quad [12a]$$

$$\begin{aligned} \text{Im}\{s_{\text{comp}}(t)\} &= \text{Im}\{s_{\text{quot}}(t) \cdot s_{\text{ideal}}(t)\} \\ &= [\text{Re}_{\text{quot}} \cdot \text{Im}_{\text{ideal}}] + [\text{Im}_{\text{quot}} \cdot \text{Re}_{\text{ideal}}] \end{aligned} \quad [12b]$$

For example, the first real point in the quotient is calculated according to Eq. [11a] by multiplying the first real points in $s_{\text{exp}}(t)$ and $s_{\text{ref}}(t)$, adding that result to the product of the first imaginary points in $s_{\text{exp}}(t)$ and $s_{\text{ref}}(t)$, and then dividing by the sum of the squares of the first real and imaginary points of $s_{\text{ref}}(t)$. There is a risk that occasional divide-by-zero conditions can occur, especially for points near the ends of the data sets where Re_{ref} and Im_{ref} both approach zero. In such cases, the denominators of Eqs. [11a] and [11b] can be set equal to their value for the previous point, or to the rms noise level in $s_{\text{ref}}(t)$, or simply to 1. The value selected normally has little effect on the final spectrum provided it lies within the noise envelope, so any reasonable choice will suffice.

Some NMR software packages provide routines for complex division but not for complex multiplication. In that case, the calculation can still be performed based on a rearrangement of Eq. [9]:

$$\begin{aligned} s_{\text{comp}}(t) &= \frac{s_{\text{exp}}(t)}{g(t)} = \frac{s_{\text{exp}}(t)}{s_{\text{ref}}(t)/s_{\text{ideal}}(t)} \\ &= \frac{s_{\text{exp}}(t) \cdot e^{-\pi \omega t}}{s_{\text{ref}}(t)/s_{\text{delta}}(t)} \end{aligned} \quad [13]$$

Figure 6 shows typical data-processing steps for reference deconvolution without using complex multiplication. First, the experimental free induction decay $s_{\text{exp}}(t)$ is acquired as usual [Fig. 6(A)]. The reference line is windowed as described above and inverse Fourier transformed, after which the resulting signal $s_{\text{ref}}(t)$ is divided by $s_{\text{delta}}(t)$ to produce the on-resonance reference signal shown in Fig. 6(B). Complex division of the original free induction decay $s_{\text{exp}}(t)$ in (A) by the on-resonance reference signal in (B) yields the result shown in Fig. 6(C). The enormous noise spikes visible in the tail of signal (C) are normal and tend to occur once signals (A) and (B) have decayed almost completely. To suppress noise in the final spectrum, data set (C) is subjected to exponential

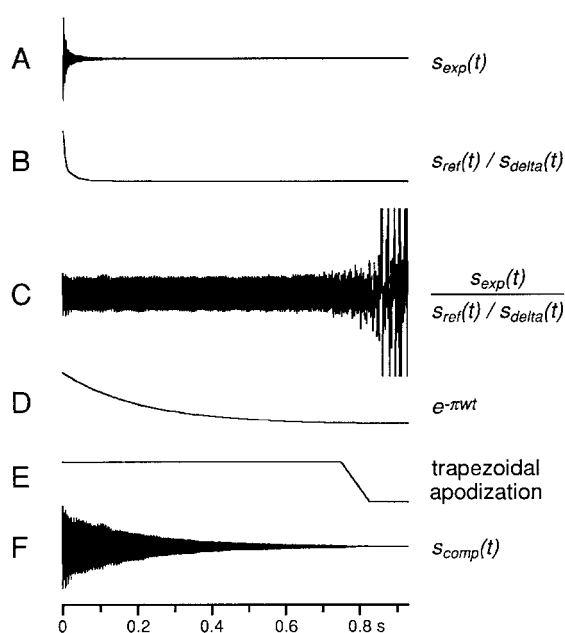


Figure 6 Steps in the reference deconvolution procedure performed without using complex multiplication. (A) Experimental FID $s_{\text{exp}}(t)$. (B) Time-domain reference signal obtained from $s_{\text{ref}}(t)/s_{\text{delta}}(t)$. This signal corresponds to the on-resonance reference peak. (C) Result of dividing $s_{\text{exp}}(t)$ shown in (A) by the reference data set in (B). (D) Exponential function $e^{-\pi w t}$ used to apodize the data set shown in (C). The parameter w is the target linewidth value. (E) Trapezoidal apodization function used to suppress noise spikes in the tail of the data set in (C). (F) Final compensated FID $s_{\text{comp}}(t)$ resulting from multiplication of the data set in (C) by the apodization functions in (D) and (E). FT of this FID yields the final compensated spectrum $S_{\text{comp}}(f)$. Comparing the compensated data (F) with the original FID (A) shows that resolution enhancement has been achieved.

multiplication (D) using a target linewidth of w Hz. Where necessary, trapezoidal apodization (E) can also be applied to eliminate any residual noise spikes in the tail without measurably affecting the final linewidths or shapes. The resulting time-domain signal $s_{\text{comp}}(t)$ shown in Fig. 6(F) is Fourier transformed to produce the final reference-deconvolved spectrum $S_{\text{comp}}(f)$. Although this procedure differs from the one outlined above, it is mathematically equivalent and employs no complex multiplication. An advantage is that once signal (C) has been calculated, it can be stored and repeatedly subjected to various combinations of exponential, trapezoidal, or other apodization to produce the desired resolution and S/N in the spectrum.

Regardless of which computational procedure is used, the value used for the target linewidth w should be no smaller than the difference between the natural linewidths of the reference peak and the spectrum of interest:

$$w \geq (\pi T_{2,\text{ref}})^{-1} - (\pi T_{2,\text{spec}})^{-1} \quad [14]$$

where $(\pi T_2)^{-1}$ is the natural linewidth in Hertz, “ref” signifies the reference line, and “spec” refers to the spectrum of interest. This constraint is essential to prevent peaks in the final deconvolved spectrum $S_{\text{comp}}(f)$ from having negative widths. Since the natural linewidths often are not known, w must usually be chosen by trial and error. Fortunately, this is not difficult in practice because if Eq. [14] is violated, the peaks will exhibit profound anomalies which disappear once a suitably large w value is used. Equation [14] also shows that it is possible to perform reference deconvolution even if the reference peak is broader than the signals in the spectrum of interest.

Choosing a suitable reference line is crucial to the practical success of reference deconvolution. Ideally, it will be a single well-resolved peak without significant underlying multiplet structure. The S/N for the reference should be as high as possible to minimize noise in the final result. An intense solvent peak is often a good choice for this reason, although caution must be used to avoid radiation damping which might change the shape of the solvent line without simultaneously affecting the other peaks. The reference line may be part of the spectrum of interest, or it can be recorded in a separate acquisition. If the reference signal is acquired separately, both data sets

should have the same digital resolution in ppm/point. When the reference is part of the spectrum of interest, it must be very well separated from the other signals in the spectrum. This is necessary partly so the windowing operation does not truncate the peak, which would introduce artifacts into the deconvolved spectrum. Figure 7 shows that truncation is greater in the imaginary part (dispersion mode) of $S_{\text{ref}}(f)$ than in its real part (absorption mode) because $\text{Re}\{S_{\text{ref}}(f)\}$ tends to zero asymptotically as $1/f^2$, whereas $\text{Im}\{S_{\text{ref}}(f)\}$ tends to zero asymptotically as $1/f$. In practice, truncation of the real part is usually easy to avoid, but it can be severe for the imaginary component of the data. One solution to the problem is to extrapolate the dispersion wings of the imaginary part to the edges of the spectrum. However, this involves some form of curve fitting, which is not only cumbersome but can easily lead

to artifacts if not properly implemented. A more elegant solution is simply to discard the imaginary data and use the real part of the spectrum to generate the imaginary part via the Hilbert transform, expressed mathematically as:

$$\text{Im}\{S(\omega)\} = -\frac{1}{\pi} \int_{-\infty}^{\infty} \frac{\text{Re}\{S(\omega')\}}{\omega - \omega'} d\omega' \quad [15]$$

Many mathematical packages have a function that performs the Hilbert transform. Alternatively, an indirect Hilbert transform can be incorporated into the reference peak selection process as follows (12): zero-pad the experimental FID $s_{\text{exp}}(t)$ to twice its size, apply a complex FT to the zero-padded data, window the real part of the resulting spectrum to select the reference line, zero the entire imaginary part of the spectrum,

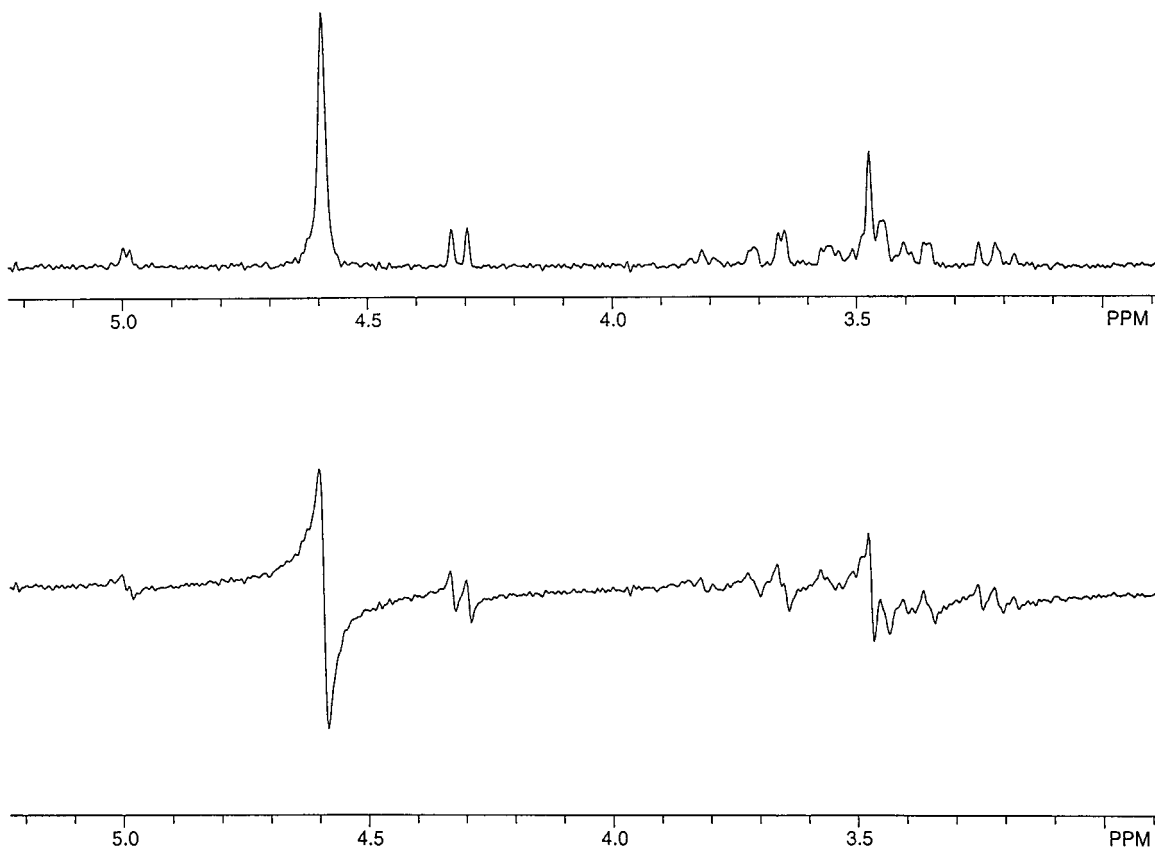


Figure 7 Proton NMR spectrum of galactose in D_2O showing the real component (top) and imaginary component (bottom). The HOD singlet (4.6 ppm) in the real part of the spectrum appears to be well resolved and suitable for use as the reference for deconvolution. However, the imaginary component of the signal is considerably less well resolved owing to its extended dispersion-mode “wings.” The application of a simple windowing function to both the real and imaginary parts could produce serious truncation artifacts in the imaginary data.

perform an inverse complex FT, and discard the second half of both the real and imaginary time-domain data. It should be noted that since $s_{\text{exp}}(t)$ is Fourier transformed before the imaginary spectrum is zeroed, the reference peak S/N is not degraded by this procedure.

In the discussion of reference deconvolution so far, the final target line shape in the frequency domain has been assumed to be Lorentzian (i.e., the apodization function in the time domain is a decaying exponential), as shown in Fig. 6(D). There are, however, a large number of other apodization functions that could be applied at this stage. One of the most common ones, which is used for resolution enhancement, is the Lorentzian-Gaussian transformation (29, 30). This can be described mathematically as multiplication in the time domain by a factor $h(t)$:

$$h(t) = e^{t/a} \cdot e^{-t^2/b} \quad [16]$$

where the first term in $h(t)$ represents resolution enhancement via multiplication with a positive exponential, and the second transforms the line shape to a Gaussian. The resulting line shape is

narrower at the base than a Lorentzian, but it is important to recognize that peaks with low intensities or large linewidths may be lost, meaning that correct integration of the spectrum is no longer possible.

One final point of note is the possibility of the reference peak being split and containing significant doublet character. This is most commonly encountered in a missetting of the odd-order z shims in high-resolution NMR spectroscopy. If the two “components” of the split peak have similar amplitudes, then the magnitude of $s_{\text{ref}}(t)$, the divisor in Eqs. [11a] and [11b], contains points of near-zero amplitude at certain time points. Depending upon the S/N, this can result in large artifacts in the final spectra processed by reference deconvolution, and may indeed preclude its use. The problems associated with this phenomenon are shown in Fig. 8, where the single resonance shown in (A) experiences a progressively more pronounced split field in (B–D). The FIDs, shown in (E–H), contain a correspondingly larger number of zero crossings, which also occur at earlier time points in the FID. Each zero crossing in the reference FID has the potential to

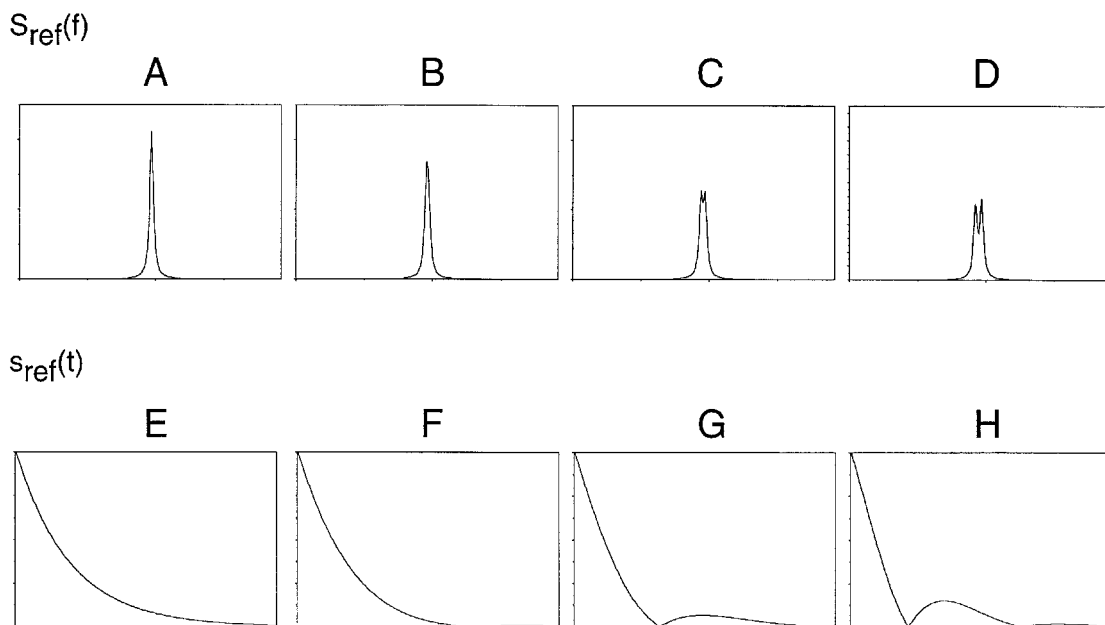


Figure 8 Simulated spectra showing the effects of a “split-field” on $s_{\text{ref}}(t)$. (A) Single nonsplit resonance line with a width of 3 Hz. (B–D) Increasing doublet character is introduced into the line, with splitting between the two components being 1.5, 3, and 4.5 Hz. (E–H) Corresponding time-domain FIDs produced by inverse Fourier transformation of (A–D), respectively. The data, shown in magnitude mode, correspond to the divisor in Eqs. [11a] and [11b]. Zero values occur more often, and at earlier time points in the FID, with increased peak splitting. Significant artifacts could be introduced into compensated spectra produced using $s_{\text{ref}}(t)$ in (G) and (H).

produce a large anomalous spike at the corresponding point in the final FID. It is therefore clear that shims producing badly split lines should be avoided if the use of reference deconvolution is anticipated.

HOMONUCLEAR REFERENCE DECONVOLUTION

In many applications, the reference line and the spectrum of interest represent the same detected nucleus (e.g., protons), and the signals are often acquired simultaneously. Several examples of this homonuclear reference deconvolution method are described here, beginning with high-resolution data acquired using optimized shim settings. Even in such cases, it is often possible to improve the resolution by deconvolving to remove the effects of small residual field inhomogeneities. This is demonstrated in Fig. 9 for proton spectra of 3-chlorobenzophenone in a mixture of CDCl_3 and

CH_2Cl_2 . The nine strongly coupled aromatic protons in this compound produce a spectrum [Fig. 9(A)] containing a multitude of peaks that are not fully resolved. Deconvolution using the singlet resonance of dichloromethane (5.3 ppm; not shown) as the reference produced the spectrum shown in Fig. 9(B). The deconvolved spectrum shows greatly improved resolution which allows scalar coupling patterns to be seen more clearly. This is even more apparent in expansions [spectra (C) and (D)], where deconvolution reveals several peaks which were totally obscured in the original spectrum.

If a particularly small sample volume is used, either to achieve a high concentration and better S/N or to improve the rf field homogeneity over the sample, then considerable line shape distortions can occur, as discussed previously. An example of this is shown in Fig. 10 for a methyl salicylate sample that was confined fully inside the sensitive region of the 5-mm-diameter coil. Despite spinning, the proton spectrum [Fig. 10(A)] exhibited poor resolution and line shapes. Reference deconvolution improved the linewidths and,

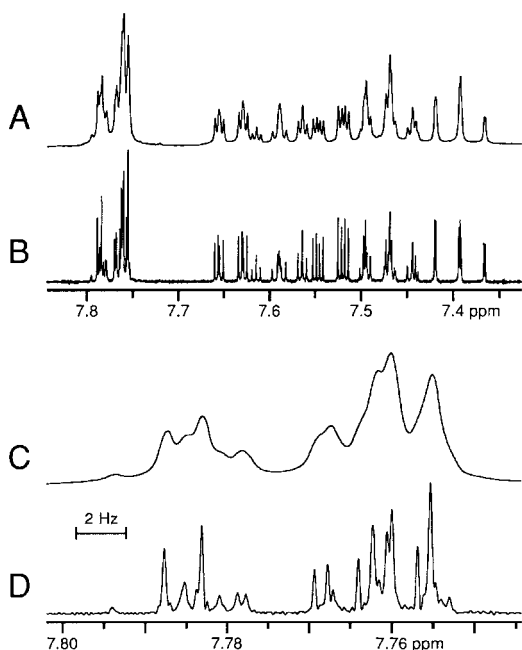


Figure 9 Proton NMR spectra (300 MHz) of 3-chlorobenzophenone in a mixture of CDCl_3 and CH_2Cl_2 . The sample was contained in a spinning 5-mm NMR tube. (A) Normal spectrum obtained without time-domain apodization. (B) Deconvolved spectrum using the CH_2Cl_2 peak as the reference and a target Lorentzian linewidth of 0.05 Hz. Expansions of the normal (C) and deconvolved (D) spectra reveal the great detail which deconvolution provides, including peaks which were completely obscured in the normal spectrum.

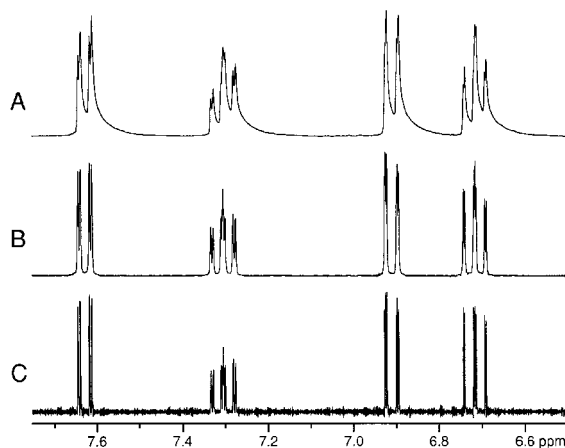


Figure 10 Proton NMR spectra (300 MHz) of neat methyl salicylate in a spinning 5-mm tube (aromatic region shown). The cylindrical sample was smaller than the rf coil volume. The normal spectrum (A) processed without time-domain apodization exhibited heavily distorted line shapes owing to the sample/glass/air interfaces present inside the sensitive region of the probe. Deconvolution using the methyl peak as the reference produced greatly improved line shapes (B,C). When a target Lorentzian line width of 0.52 Hz was used (B), the methyl peak S/N remained the same as in the original spectrum (A). A smaller target line width of 0.15 Hz gave baseline resolution for many peaks (C) but also a sixfold loss in S/N compared to spectrum (A).

especially, the shapes [Fig. 10(B)]. Significantly, the S/N was the same for spectra (A) and (B), as measured using the intensity of the well-resolved singlet methyl peak near 3.7 ppm. (Note that the overlapping lines shown in Fig. 10 do not provide fair comparisons of S/N variations, since resolution improvements also reduce the apparent signal intensities solely because the overlap decreases.) By using a small target linewidth, deconvolution can also produce a spectacular resolution improvement, albeit with a substantial S/N penalty [Fig. 10(C)]. This is even more evident in an expansion of the multiplet near 7.3 ppm, where 15 of the 16 peaks expected from first-order coupling are visible (Fig. 11). The two center lines of the pattern overlap and remain unresolved.

As discussed previously, another situation in which line shapes can be dominated by the effects of magnetic field inhomogeneity is when the sample is not spinning. Figure 12 shows the dramatic improvements that reference deconvolution can

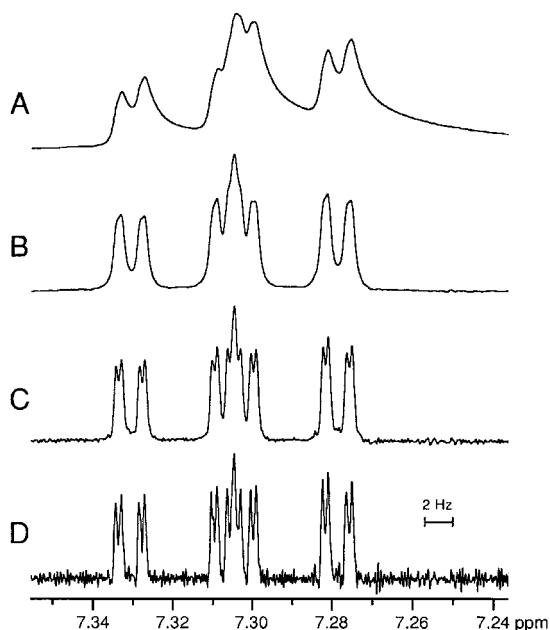


Figure 11 Expansion of the methyl salicylate proton multiplet near 7.3 ppm (see Fig. 10). (A) Original spectrum. (B) Deconvolved spectrum using the methyl peak as the reference and a target Lorentzian line width of 0.52 Hz. The S/N for the methyl peak was the same as in the original spectrum. (C) Deconvolved spectrum using a target line width of 0.25 Hz. The S/N was threefold lower than in the original spectrum. (D) Deconvolved spectrum using a target linewidth of 0.10 Hz. The S/N was decreased by ninefold relative to the original spectrum. All the predicted lines are resolved except for the two in the center of the pattern.

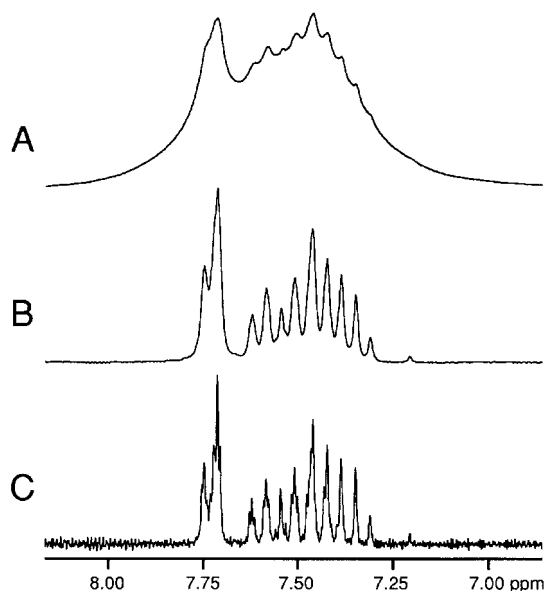


Figure 12 Proton spectra (200 MHz) of a mixture of 3-chlorobenzophenone and tetramethylsilane (TMS) in CDCl_3 . Only the aromatic region is shown. The large (2.6 cm long \times 1.8 cm diameter) sample was contained in a nonspinning vial and was smaller than the solenoidal rf coil. (A) Original spectrum with no time-domain apodization; TMS S/N = 5210:1. (B) Deconvolved spectrum using the TMS peak as the reference and a target Lorentzian linewidth of 2.2 Hz. TMS S/N = 5400:1. (C) Deconvolved spectrum using a target linewidth of 0.75 Hz. TMS S/N = 1180:1.

produce in this case. The measurement was performed using a 31-cm-bore horizontal magnet designed mainly for imaging and spectroscopy of animals. Deconvolution reduced many of the deleterious effects of field inhomogeneity and converted the rather featureless spectrum of Fig. 12(A) into something much more informative [Figs. 12(B) and 12(C)] even approaching the resolution that might be anticipated from a conventional high-resolution spectrometer.

Another case in which spinning is usually not possible is when solenoidal microcoils are used to detect very small sample masses. These coils have remarkably high sensitivities, but since the metal conductor is extremely close to the sample (typically $< 100 \mu\text{m}$ away), spectral distortions can occur owing to magnetic susceptibility differences (20). An example is shown in Figure 13, where considerable line distortion and broadening are evident in the spectrum. Much better line shapes and resolution result from deconvolution using the residual protonated solvent signal as the reference.

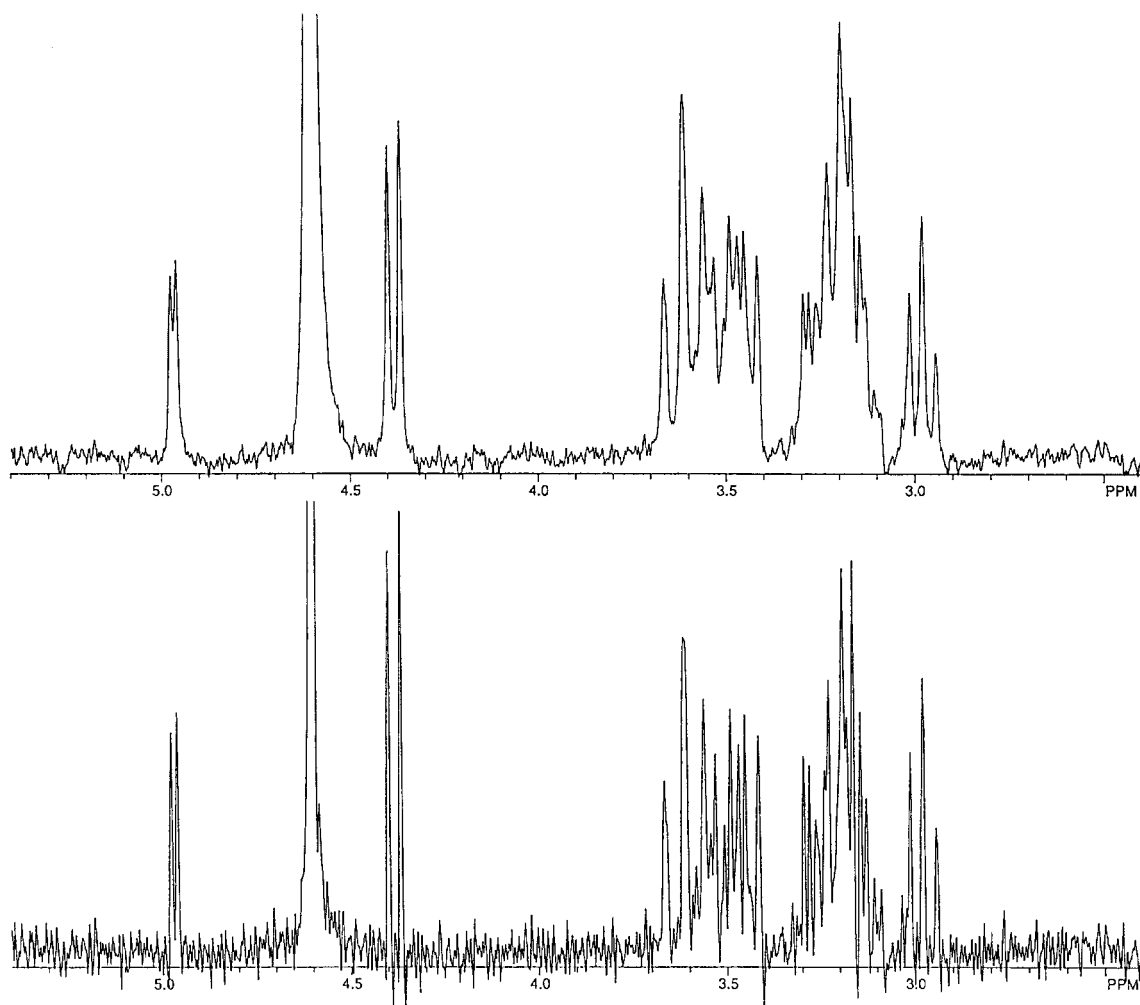


Figure 13 Proton NMR spectra (250 MHz) of sucrose in D_2O obtained using a solenoidal rf microcoil of diameter $350\ \mu\text{m}$. The sample was contained within a capillary of inner diameter $250\ \mu\text{m}$ and was not spinning. (A) Original spectrum. (B) Deconvolved spectrum using the residual HOD peak as the reference.

One further case of severe line broadening will be considered: that of a sample containing a paramagnetic or ferromagnetic component. This often results in broadening alone without accompanying peak asymmetry. In the example shown in Fig. 14(A), ferric oxide particles suspended in a tri-*n*-butyl phosphate solution make the linewidths so large that fine scalar couplings are obscured. Most of this information can be regained using reference deconvolution [Fig. 14(B)], as can be seen by comparing with a normal high-resolution spectrum of an uncontaminated sample [Fig. 14(C)].

The deconvolved spectra of Fig. 12 were produced by using the internal tetramethylsilane (TMS) signal as the reference. The TMS line is

convenient for this purpose, but its use is often complicated by the presence of small ^{29}Si and ^{13}C satellites flanking the central peak at ± 3.3 and ± 59 Hz, respectively. Since the reference line is supposed to be representative of all peaks in the spectrum, any fine structure which is unique to the reference should generally be removed before deconvolution is performed. In the case of TMS, the ^{13}C satellites are usually eliminated during the initial windowing operation, but the ^{29}Si sidebands are more problematic owing to their close proximity to the central peak. For the spectra of Fig. 14, they were removed manually by adjusting the values of individual points in the real frequency-domain TMS spectrum prior to Hilbert transformation. This method is straightforward,

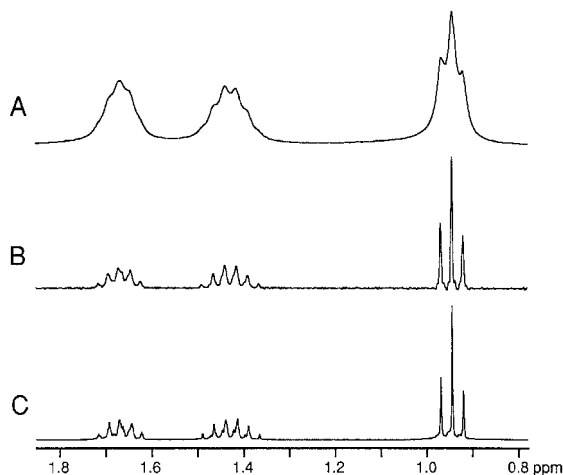


Figure 14 Proton NMR spectra (300 MHz) of tri-*n*-butyl phosphate in CDCl_3 containing TMS and contaminated with ferric oxide powder. A spinning 5-mm tube was used. TMS and downfield multiplet signals are not shown. (A) Original spectrum obtained after extensive shimming. The TMS line width was 5.8 Hz. (B) Deconvolved spectrum using TMS as the reference peak. (The TMS ^{29}Si sidebands were removed prior to calculations.) Deconvolution produced much clearer scalar coupling patterns. (C) Normal spectrum obtained in the absence of ferric oxide.

but is also tedious and subjective since the operator must estimate how the spectrum would appear in the absence of the satellites. A more elegant approach would be to decouple ^{29}Si during data acquisition or to employ an automated fitting algorithm to estimate the baseline under the satellites. With very noisy or badly broadened spectra (e.g., Fig. 12), the fine structure can generally be ignored, and the entire TMS signal envelope is used as the reference. Unlike satellites due to scalar coupling, spinning sidebands affect the reference and other spectral peaks equally, so they can be removed from the final result by including them in the reference spectrum.

Although narrow lines are obviously desirable for accurate measurements of chemical shifts and scalar coupling constants, they are also important for the determination of relaxation times. Peak overlap can lead to erroneous T_1 or T_2 measurements, especially when the overlapped signals arise from spins having very different relaxation rates. This problem is often most intractable for inversion-recovery T_1 data, where adjacent peaks may have opposite phases, resulting in partial signal cancellation and uncertainty in the baseline position (31). Accurate peak information can, in

principle, be extracted from such spectra by line fitting, but this method is laborious and may be impractical if the lines are badly distorted. It is clearly better to optimize the resolution and line shapes before measuring the signal areas or intensities. Since reference deconvolution is a linear process (i.e., relative signal areas are unaffected), it can safely be used to enhance resolution in such data sets. Furthermore, even very distorted peaks are converted into Lorentzians, which enables accurate line fits to be performed, if necessary, for any signals which remain overlapped. Figure 15 shows the result of deconvolving an inversion-recovery spectrum of 3-chlorobenzophenone using a solvent line as the reference. Peak overlap is reduced in the deconvolved spectrum, and the baseline is very clearly defined. The excellent resolution also enables some signal integrals to be measured directly, which was not possible with the original spectrum.

Despite the successes shown above, it is important to recognize that reference deconvolution offers little resolution enhancement if the linewidths are determined almost completely by the natural T_2 values. In fact, if $T_2 = T_2^*$, the reference deconvolution technique reduces mathematically to the conventional exponential multiplication approach and performs no better. Figure 16 shows a portion of the 300-MHz high-resolution spectrum of cholesterol in CDCl_3 before and

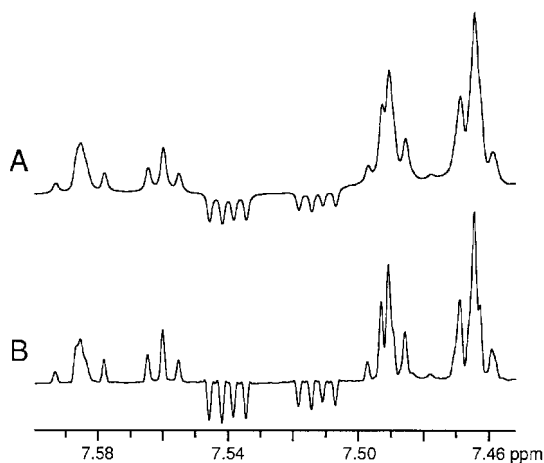


Figure 15 Proton inversion-recovery spectra (300 MHz) of 3-chlorobenzophenone in 9:1 (v/v) $\text{CDCl}_3/\text{CH}_2\text{Cl}_2$ at 25°C. The delay between the 180° and 90° pulses was 2.3 s. (A) Original spectrum (spinning) with no time-domain apodization. (B) Deconvolved spectrum using the CH_2Cl_2 peak as the reference. Note improved resolution and straight baseline following deconvolution.

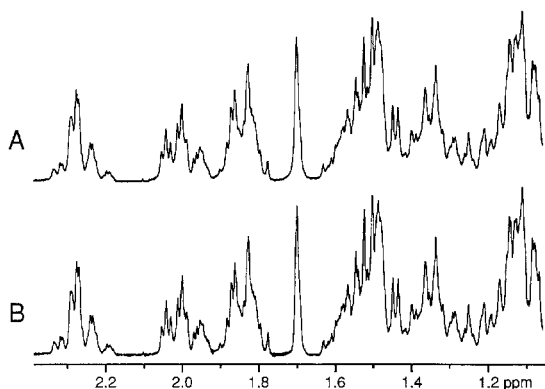


Figure 16 Proton NMR spectra (300 MHz) of cholesterol in CDCl_3 containing tetramethylsilane (TMS). A spinning 5-mm NMR tube was used, and the field was well shimmed. (A) Normal spectrum with no time-domain apodization. (B) Deconvolved spectrum using the TMS peak as the reference and a target Lorentzian line width of 0.4 Hz. The ^{29}Si sidebands were removed manually from the TMS line before the calculation was performed. Since the linewidths of the original spectrum (A) are essentially T_2 rather than T_2^* limited, there is no improvement in resolution when reference deconvolution is used.

after deconvolution using TMS as the reference. No measurable improvement occurred because the broadening effects of magnetic field inhomogeneity were small compared to the natural linewidths.

HETERONUCLEAR REFERENCE DECONVOLUTION

All the examples shown so far have employed a reference line which was part of the spectrum to be deconvolved. However, heteronuclear reference deconvolution can also be performed (for example, by using a solvent proton line as the reference to deconvolve a ^{31}P or ^{13}C spectrum acquired from the same sample). This approach actually has several advantages compared to the homonuclear case. First, if the reference spectrum contains only a single line, then the windowing step of the calculation may be unnecessary. The reference line can also be placed on resonance, avoiding the computational step of shifting it to zero frequency by deconvolution with a delta function. Next, if a solvent peak is used as the reference, its S/N is likely to be quite high, so little noise is introduced by the calculation into the final spectrum. Finally, a solvent signal is

typically acquired anyway as part of the shimming process, so instead of discarding that signal, it takes little extra time to save it for use as a reference.

Certain experimental precautions should be observed when performing heteronuclear reference deconvolution. First, the reference line and the other signals must arise from the same spatial region in the sample. In the worst case, this will force the same rf coil, tip angles, and saturations to be used for both nuclides, although some or all of these constraints may be eased depending on the details of the coil and sample arrangement. Second, the reference spectrum and spectrum of interest should be acquired using the same digital resolution in ppm/point, as mentioned previously. This is most easily accomplished by using the same number of points and spectral width in ppm for both data sets. The latter condition demands that the relative spectral widths in Hertz be scaled in proportion to the magnetogyric ratios of the two nuclides. Exact scaling will usually be prevented by finite resolution of the spectrometer's timing hardware, but the two spectral widths in ppm can still be matched to within 0.1% or so, which is adequate for all practical purposes.

An example of heteronuclear reference deconvolution is shown in Figure 17 for an aqueous solution of orthophosphate, pyrophosphate, and tripolyphosphate. The water proton line in this nonspinning sample was broad and distorted [Fig. 17(A)]. Comparison with the ^{31}P singlet of orthophosphate at 0 ppm [Fig. 17(B)] shows the line shapes to be essentially identical, strong evidence that magnetic field inhomogeneity effects were dominant in both spectra. Spectrum (C) shows the result of enhancing the resolution of spectrum (B) by exponential multiplication using a -0.5 Hz line-broadening parameter. As expected, the linewidths improved slightly but the S/N was seriously degraded. On the other hand, reference deconvolution produced extremely narrow ^{31}P lines for the same sacrifice in S/N [spectrum 17(D)]. Deconvolution using a larger target linewidth [Fig. 17(E)] produced superior line shapes and widths, as well as the same S/N as in the original spectrum. Finally, using an even larger target linewidth gave a spectrum (F) having resolution roughly comparable to that of the original data (B), but with improved line shapes and nearly threefold better S/N.

The excellent results of Fig. 17 suggest the heteronuclear deconvolution technique may perform well even when challenged by extremely

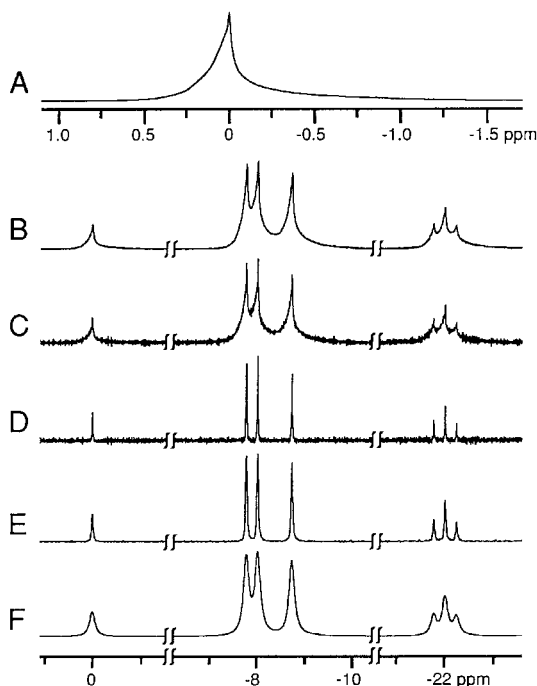


Figure 17 Demonstration of heteronuclear reference deconvolution using an aqueous solution of orthophosphate, pyrophosphate, and triphosphate (all as sodium salts) at 4.7 T. The nonspinning, cylindrical sample was 3.4 cm long \times 2.3 cm diameter and was contained completely within the rf field of a large, tunable concentric loop-gap resonator (42). ^1H and ^{31}P spectra were acquired using 45° rf pulses and 16K time-domain points. The spectral widths were 14,836.8 Hz (74.091 ppm) for ^1H and 6002.4 Hz (74.049 ppm) for ^{31}P . A. normal 200-MHz proton spectrum showing a distorted $^1\text{H}_2\text{O}$ line shape with FWHM = 25 Hz (0.12 ppm) and S/N = 14,300:1. (B) Normal 81 MHz ^{31}P spectrum obtained without time-domain apodization. For the orthophosphate (P_i) singlet at 0 ppm, FWHM = 8.2 Hz and S/N = 44:1. (C) Same as spectrum (B) except resolution enhanced by exponential multiplication using a line-broadening parameter of -0.5 Hz. P_i FWHM = 6.0 Hz, and S/N = 12:1. (D) Deconvolved ^{31}P spectrum using the proton peak (A) as the reference and a Lorentzian target linewidth of 1.0 Hz. P_i FWHM = 0.95 Hz and S/N = 12:1. (E) Same as spectrum (D) except using a target linewidth of 2.9 Hz. P_i FWHM = 3.1 Hz and S/N = 45:1. (F) Same as spectrum (D) except using a target linewidth of 11.5 Hz. P_i FWHM = 11.1 Hz and S/N = 125:1.

poor field homogeneity. This was tested (Fig. 18) for the same sample by intentionally degrading the shim, using the $^1\text{H}_2\text{O}$ FWHM as a direct measure of the homogeneity. For each shim setting, the target linewidth used during processing was adjusted to yield the same orthophosphate

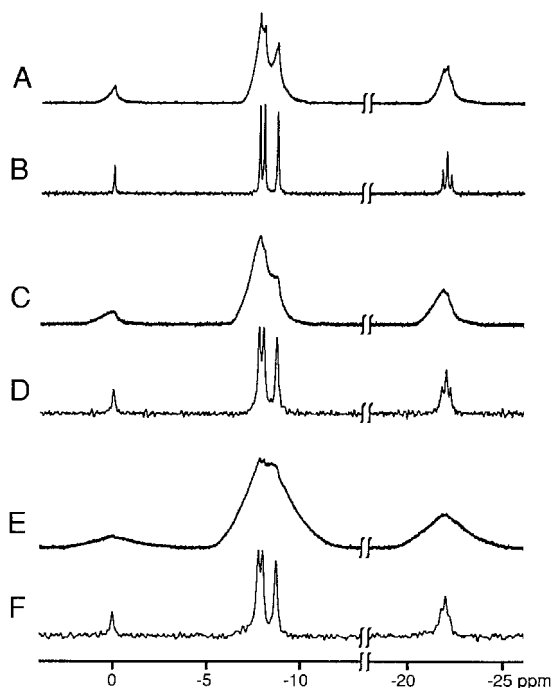


Figure 18 Performance of reference deconvolution in the presence of severe magnetic field inhomogeneity. Using the aqueous phosphate sample and conditions of Fig. 17, the shim was intentionally degraded to produce increasingly poor spectra. The field homogeneity was determined from the $^1\text{H}_2\text{O}$ FWHM, and that peak was used as the reference for ^{31}P deconvolution. Normal spectra were produced without time-domain apodization. Deconvolutions were performed using target Lorentzian linewidths adjusted to yield the same orthophosphate (P_i) S/N as in the corresponding normal spectra. (A,B) Normal and deconvolved ^{31}P spectra for $^1\text{H}_2\text{O}$ FWHM = 87 Hz (0.44 ppm). P_i FWHM = 32.5 and 6.1 Hz, respectively. P_i S/N = 18.0:1. (C,D) Normal and deconvolved ^{31}P spectra for $^1\text{H}_2\text{O}$ FWHM = 191 Hz (0.96 ppm). P_i FWHM = 74 and 15.0 Hz, respectively. P_i S/N = 10.2:1. (E,F) Normal and deconvolved ^{31}P spectra for $^1\text{H}_2\text{O}$ FWHM = 446 Hz (2.23 ppm). P_i FWHM = 183 and 15.6 Hz, respectively. P_i S/N = 8.4:1 [using four times as many averages as for spectra (A–D) to enhance visibility].

S/N both before and after deconvolution. Even for the most egregious case where the inhomogeneity exceeded 2 ppm, deconvolution easily revealed the correct number of signals and at least hinted at their scalar coupling patterns [Figs. 18(E) and 18(F)]. ^{31}P linewidths and shapes in the deconvolved spectra improved markedly compared to those in the original spectra with equivalent S/N. Figures 17 and 18 also demonstrate the effect of field homogeneity on S/N. $^1\text{H}_2\text{O}$ FWHM values of 0.12, 0.44, 0.96, and 2.23 ppm produced

orthophosphate S/N of 44:1, 18:1, 10:1, and 4.2:1, respectively, for equal numbers of averages. As expected, the S/N decreased with increasing linewidth, although the dependence was not linear owing to changes in the line shape. In each case, deconvolution efficiently restored most of the lost resolution, but it did not recover the S/N losses. The lesson of these experiments is clear: there is no substitute for a good shim. However, once the best practical shim has been obtained, deconvolution can be very effective for suppressing the effects of any remaining inhomogeneities on the spectral resolution.

The success of reference deconvolution does not rely on high rf field homogeneity. Consequently, the technique can be used with surface coils provided that the reference line and spectrum of interest both arise from the same spatial region of the sample. In most experiments, that condition will be satisfied if the spectrum also contains the reference line or, for heteronuclear studies, if the same coil and nutation angles are used for both nuclides. The compatibility of deconvolution with data acquired using surface coils is potentially an advantage for *in vivo* measurements where the linewidths are invariably dominated by magnetic field inhomogeneity effects. Figure 19 shows proton and ^{31}P spectra obtained from the abdomen of an anesthetized rat at 4.7 tesla. The proton spectrum [Fig. 19(A)] was typical, exhibiting broad signals due to tissue water and lipids. To prepare it for use as a heteronuclear reference, the spectrum was windowed to remove the lipid peaks, leaving only the distorted water line [Fig. 19(B)]. Deconvolving this from the normal ^{31}P spectrum [Fig. 19(C)] narrowed the lines significantly, although the improvement was accompanied by a loss in S/N [Fig. 19(D)]. A small signal due to NAD^+ and NADH was revealed which was not visible in the original spectrum.

In this instance, the benefits of deconvolution were not as dramatic as for the *in vitro* examples shown previously. This would result if a pulse-width calibration error caused the proton and ^{31}P spectra to originate from somewhat different spatial regions, making their line shapes different. However, *in vivo* spectra acquired using homogeneous rf coils have also been found to improve only marginally after deconvolution (data not shown). The reason may well be microheterogeneities in the tissue itself, since much of the water is extracellular, whereas the metabolites are mainly confined to the cytoplasm and proba-

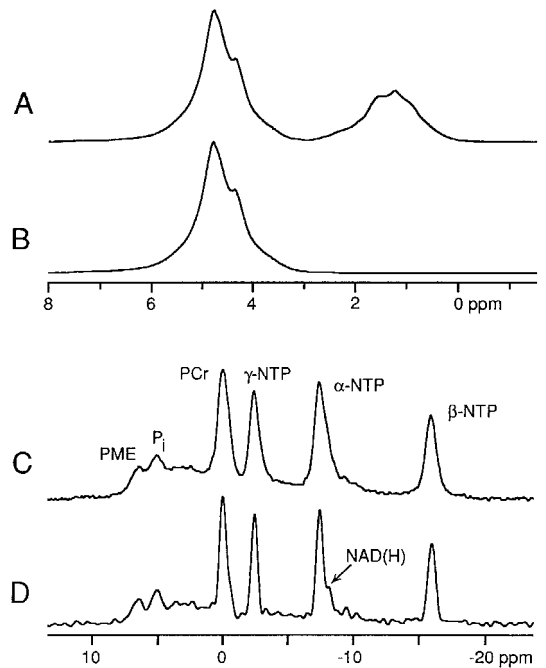


Figure 19 Application of heteronuclear reference deconvolution to *in vivo* NMR. Proton and ^{31}P spectra were acquired at 4.7 T from the abdominal muscle and underlying liver of an anesthetized rat using a 1.2-cm-diameter surface coil. (A) Proton spectrum exhibiting typical broad lipid and water peaks near 1 and 5 ppm, respectively. (B) Proton spectrum after windowing to remove the lipid signals. (C) Normal ^{31}P spectrum containing peaks for phosphomonoesters (PME), orthophosphate (P_i), phosphocreatine (PCr), and nucleoside triphosphates (NTP). Time-domain exponential apodization was applied using a line-broadening parameter of 10 Hz. $\beta\text{-NTP}$ S/N = 42:1. (D) Deconvolved ^{31}P spectrum using spectrum (B) as the reference and a target Lorentzian linewidth of 40 Hz. $\beta\text{-NTP}$ S/N = 26:1. A shoulder is visible owing to nicotinamide adenine dinucleotide (NAD^+) and its reduced form (NADH).

bly experience slightly different susceptibility effects. A related mechanism has been invoked to explain the mediocre performance of the technique for enhancing proton spectra of brain (32). An additional complication arises when only homonuclear instead of heteronuclear data are acquired, since it is then necessary to find a single well-resolved peak in the crowded *in vivo* spectrum to use as a reference. For ^{31}P spectra, the phosphocreatine singlet would be a logical candidate, but it virtually always overlaps adjacent peaks. The β -nucleoside triphosphate signal is often adequately resolved, but as the superposition of several underlying multiplets with slightly

different chemical shifts, it is not really suitable for use as a reference. In summary, while reference deconvolution may be beneficial for *in vivo* spectra, the application of the technique is not always straightforward, and spectacular improvements have generally not been demonstrated.

S/N PERFORMANCE OF REFERENCE DECONVOLUTION

Several of the spectra discussed above exhibit significantly better S/N following deconvolution. In some cases (e.g., Fig. 17), both the S/N and resolution improve simultaneously. At first glance, this may be disconcerting, since most spectroscopists are accustomed to an inverse relationship between S/N and linewidth when traditional time-domain apodization techniques are employed. Thus, it is natural to question the apparently exceptional performance of reference deconvolution. Comparing results of deconvolution with those obtained from other processing techniques is complicated by the fact that it is possible to produce spectra having a wide range of resolutions and signal intensities with any of these approaches. To evaluate their true relative performance, both the S/N and linewidth obtained from the various methods must be compared simultaneously (bearing in mind that deconvolution will nearly always produce a superior line shape).

Such a comparison was made for the orthophosphate ^{31}P singlet of Fig. 17. The data were first processed by conventional exponential multiplication using 13 different values of the line broadening parameter, and the resulting ^{31}P linewidths and corresponding S/N values are plotted in Fig. 20 (circles). The spectrum was then generated using Lorentzian-to-Gaussian conversion, employing -8.0 Hz line-broadening in the exponential multiplication and 16 different line-broadening values in the Gaussian multiplication. These results are also plotted in Fig. 20 (diamonds). Finally, with the $^1\text{H}_2\text{O}$ line as the reference, the spectrum was processed by reference deconvolution using 17 target Lorentzian linewidths, and the results were plotted (squares). When large line-broadening or target linewidth parameters were employed, high S/N and FWHM values were obtained, as would be expected for aggressive apodization in any of the methods. A far more interesting region is for linewidths below about 14 Hz, where the plots diverged. The performance of exponential multiplication was infe-

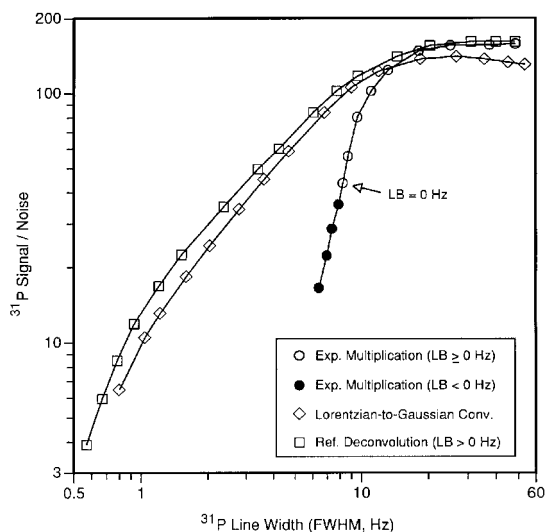


Figure 20 Plots of ^{31}P S/N versus linewidth for aqueous orthophosphate spectra processed using conventional exponential multiplication (circles), Lorentzian-to-Gaussian conversion (diamonds), and reference deconvolution (squares). The sample and conditions of Fig. 17 were used, and the $^1\text{H}_2\text{O}$ line served as the reference. Line-broadening values for exponential multiplication ranged from -0.4 to -0.1 Hz (filled circles) and 0 to $+30$ Hz (open circles). Lorentzian-to-Gaussian conversion was performed by exponential multiplication with -8.0 Hz line-broadening, followed by Gaussian multiplication with line-broadening values from $+2.6$ to $+47$ Hz. Target Lorentzian line widths for reference deconvolution ranged from $+0.2$ to $+50$ Hz. The same region of baseline was used to measure the noise in every case. These plots demonstrate that reference deconvolution outperforms exponential multiplication for resolution enhancement and that simultaneous improvements in both resolution and S/N are possible using this technique. Lorentzian-to-Gaussian conversion was also superior to exponential multiplication, giving S/N values and linewidths (but not line shapes) nearly as good as those from reference deconvolution.

rior throughout this range, and the S/N value was $< 20\%$ of those obtained by Lorentzian-to-Gaussian conversion and reference deconvolution for a linewidth of 6.5 Hz. The latter two techniques easily generated narrow lines, yielding about fivefold better resolution for $\text{S/N} = 16:1$ and a linewidth improvement of over an order of magnitude in the most extreme case. Compared to the raw unapodized spectrum, reference deconvolution and Lorentzian-to-Gaussian conversion nearly tripled the S/N for equivalent linewidth and reduced the width by over twofold for constant S/N. Both of these methods pro-

duced similar curves in Fig. 20. However, their performance differed significantly with regard to line shape. Figure 21 shows aqueous phosphate ^{31}P NMR spectra generated using these two techniques, along with results obtained by exponential multiplication. The linewidth and S/N advantages suggested by Fig. 20 are clearly evident, but it is important to note that the line shapes produced by reference deconvolution are far superior to those obtained from Lorentzian-to-Gaussian conversion even though the widths are nearly the same.

The plots of Fig. 20 confirm that it is possible to improve both the spectral resolution and S/N

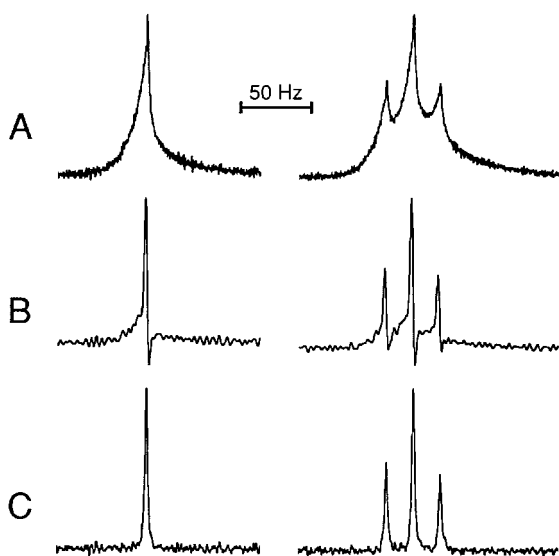


Figure 21 Comparison of ^{31}P NMR line shapes for signals processed using exponential multiplication (A), Lorentzian-to-Gaussian conversion (B), and reference deconvolution (C). The spectra were obtained using the aqueous phosphate sample and conditions of Fig. 17. Only the orthophosphate singlet (left) and tripolyphosphate triplet (right) are shown. Processing parameters were selected to produce orthophosphate S/N of 30:1 for all three methods. A line-broadening of -0.16 Hz was used for exponential multiplication. Lorentzian-to-Gaussian conversion was performed by multiplying the FID by exponential and Gaussian functions using -8.0 and $+4.1$ Hz line-broadening parameters, respectively. Reference deconvolution employed $^1\text{H}_2\text{O}$ as the reference and a target Lorentzian line width of $+2.1$ Hz. Results from simple exponential multiplication were clearly inferior to those obtained by Lorentzian-to-Gaussian conversion and reference deconvolution. However, although the latter two methods gave similar linewidths, deconvolution produced far better line shapes.

simultaneously by using reference deconvolution or Lorentzian-to-Gaussian conversion. Why does exponential multiplication perform so badly by comparison? In practice, field inhomogeneities produce a range of NMR line components having not only different widths, but, when summed together, shapes that are not Lorentzian. However, multiplying the experimental time-domain data set by any single positive exponential function always results in the removal of one Lorentzian component from the frequency-domain line. It is therefore naive to expect a satisfactory result from the exponential multiplication technique. In other words, if the wrong function is used for resolution enhancement, of course it works poorly. Lorentzian-to-Gaussian conversion offers greater flexibility in that two linewidth manipulations are performed, and the line-broadening operation tends to suppress the noise which is amplified in the tail of the FID by the line-narrowing step. Thus, this method performs better than traditional exponential multiplication with respect to both S/N and line shape. Despite this, however, Lorentzian-to-Gaussian conversion still employs just two theoretical line shape functions which may only generally resemble the major components of the actual experimental line. The result can be residual line shape distortions of the type shown in Fig. 21. If it were possible to modify these resolution enhancement techniques to use an infinite number of functions, each having its own unique shape and width, nearly perfect removal of inhomogeneous spectral line components would become possible. This, in fact, is basically what is accomplished when an experimental reference line is used to measure the distortion in the spectrum. The key to success thus lies in using the actual experimentally measured reference function instead of some convenient but erroneous hypothetical function. The additional information added to the calculation by this measurement yields not only improved S/N but also freedom from line shape distortions.

Although reference deconvolution has been found to perform comparatively well with regard to spectral S/N, it is still important that the raw data contain as little noise as practical. This is easily seen by inspection of Eq. [10], which shows that noise present in either the spectrum of interest or in the reference line will affect the final noise level in the deconvolved spectrum. Therefore, when dealing with noisy data, it may be

desirable to employ some form of denoising as an adjunct to deconvolution. Ideally, this would improve the S/N while having a negligible effect on the line shapes and widths. Wavelet denoising has recently been introduced as a possible method for accomplishing this (33).

CONCLUSIONS AND FURTHER READING

This article has shown how the relatively simple technique of reference deconvolution can be used to improve spectral resolution in applications where considerable local magnetic field homogeneities exist. The spectrum of interest and the reference spectrum can be acquired simultaneously (the homonuclear case) or, if it is more convenient, they can also be recorded separately and may even employ different nuclides (the heteronuclear case). There is a tradeoff between resolution and S/N, but a judicious choice of processing parameters can nevertheless enable chemical shifts and scalar couplings to be measured even though they might be completely hidden in the preprocessed spectrum. Furthermore, the performance of the technique with respect to S/N can be far superior to that of the exponential multiplication method, even yielding simultaneous improvements in both S/N and resolution. Whereas Lorentzian-to-Gaussian conversion may provide resolution and S/N enhancements nearly as great as those from reference deconvolution, the latter method produces better line shapes.

Reference deconvolution has recently been used for a number of other applications, particularly with two-dimensional techniques, and the work of Morris and coworkers has been pivotal in this expansion. They demonstrated the extension of the method to the reduction of t_1 artifacts in two-dimensional spectroscopy (34, 35), its application in high-resolution diffusion ordered spectroscopy (36), and the use of multiplets as reference peaks in cases where singlet peaks are either not present or are poorly resolved (37). Comprehensive reviews of these techniques can be found in Refs. 38 and 39. It should also be noted that other reference deconvolution methods have been introduced recently (40, 41).

MATLAB code for carrying out reference deconvolution can be downloaded from the following site: <http://www.mrel.beckman.uiuc/mlam/refdeconvolution>.

REFERENCES

1. Chmurny GN, Hoult DI. The ancient and honourable art of shimming. *Concepts Magn Reson* 1990; 2:131–149.
2. Doty FD, Entzminger G, Yang YA. Magnetism in high-resolution NMR probe design. I: General methods. *Concepts Magn Reson* 1998; 10: 133–156.
3. Doty FD, Entzminger G, Yang YA. Magnetism in high-resolution NMR probe design. II: HR MAS. *Concepts Magn Reson* 1998; 10:239–260.
4. Biraud YG. Les méthodes de déconvolution et leurs limitations fondamentales. *Rev Phys Appl* 1976; 11:203–214.
5. Wouters JM, Petersson GA. Reference line shape adjusted difference NMR spectroscopy. I. Theory. *J Magn Reson* 1977; 28:81–91.
6. Wouters JM, Petersson GA, Agosta WC, Field FH, Gibbons WA, Wyssbrod H, Cowburn D. Reference line shape adjusted difference NMR spectroscopy. II. Experimental verification. *J Magn Reson* 1977; 28:93–104.
7. Taquin J. Line-shape and resolution enhancement of high-resolution F.T.N.M.R. in an inhomogeneous magnetic field. *Rev Phys Appl* 1979; 14:669–681.
8. Morris GA. Compensation of instrumental imperfections by deconvolution using an internal reference signal. *J Magn Reson* 1988; 80:547–552.
9. Morris GA, Cowburn D. Suppression of artefacts in nuclear Overhauser effect difference spectroscopy by reference deconvolution. *Magn Reson Chem* 1989; 27:1085–1089.
10. de Graaf AA, van Dijk JE, Bovée WMMJ. QUALITY: Quantification improvement by converting line shapes to the Lorentzian type. *Magn Reson Med* 1990; 13:343–357.
11. Green DVS, Hillier IH, Morris GA, Whalley L. Determination of the barrier to C–N bond rotation in captopril: application of reference deconvolution to line-shape analysis. *Magn Reson Chem* 1990; 28:820–823.
12. Gibbs A, Morris GA. Reference deconvolution: Elimination of distortions arising from reference line truncation. *J Magn Reson* 1991; 91:77–83.
13. Metz KR. Simple technique for improving resolution in heteronuclear NMR spectra by deconvolution with the measured B_0 field distribution. 35th Experimental NMR Conference, Asilomar, CA; 1994. p 264.
14. Metz KR. NMR resolution enhancement with minimal signal/noise losses. 36th Experimental NMR Conference, Boston, MA; 1995. p 241.
15. Metz KR. Signal-to-noise performance of resolution enhancement techniques. 38th Experimental NMR Conference, Orlando, FL; 1997. p 88.

16. Lam MM, Webb AG. Signal to noise and resolution analysis of the reference deconvolution method in NMR spectroscopy. 38th Experimental NMR Conference, Orlando, FL; 1997. p 92.
17. Fuks LF, Huang FSC, Carter CM, Edelstein WA, Roemer PB. Susceptibility, line shape, and shimming in high-resolution NMR. *J Magn Reson* 1992; 100:229–242.
18. Bhagwandien R, van Ee R, Beersma R, Bakker CJG, Moerland MA, Lagndijk JJW. Numerical analysis of the magnetic field for arbitrary magnetic susceptibility distributions in 2D. *Magn Reson Imag* 1992; 10:299–313.
19. Soffe N, Boyd J, Leonard M. The construction of a high-resolution 750 MHz probehead. *J Magn Reson A* 1995; 116:117–121.
20. Webb AG, Grant SG. Signal-to-noise and magnetic susceptibility trade-offs in solenoidal microcoils for NMR. *J Magn Reson B* 1996; 113:83–87.
21. Zelaya FO, Crozier S, Dodd S, McKenna R, Doddrell DM. Measurement and compensation of field inhomogeneities caused by differences in magnetic susceptibility. *J Magn Reson B* 1995; 115:131–136.
22. Arnold JT. Magnetic resonance of protons in ethyl alcohol. *Phys Rev* 1956; 102:136–150.
23. Cox IJ, Bydder GM, Gadian DG, Young IR, Proctor E, Williams SR, Hart I. The effect of magnetic susceptibility variations in NMR imaging and NMR spectroscopy *in vivo*. *J Magn Reson* 1986; 70:163–168.
24. Chung H-W, Hwang SN, Yeung HN, Wehrli FW. Mapping of the magnetic-field distribution in cancellous bone. *J Magn Reson B* 1996; 113:172–176.
25. Bertolina JA, Durney CH, Ailion DC, Cuttillo AG, Morris AH, Goodrich KC. Experimental verification of inhomogeneous line-broadening calculations in lung models and other inhomogeneous structures. *J Magn Reson* 1992; 99:161–169.
26. Fabry ME, San George RC. Effect of magnetic susceptibility on nuclear magnetic resonance signals arising from red cells: A warning. *Biochem* 1983; 22:4119–4125.
27. Ernst RR, Freeman R, Gestblom B, Lusebrink TR. Detection of very small N.M.R. spin coupling constants by resolution enhancement. *Mol Phys* 1967; 13:283–286.
28. Clouse AO, Moody DC, Rietz RR, Roseberry T, Schaeffer R. Application of line narrowing to ^{11}B nuclear magnetic resonance spectra. *J Am Chem Soc* 1973; 95:2496–2501.
29. Ferrige AG, Lindon JC. Resolution enhancement in FT NMR through the use of a double exponential function. *J Magn Reson* 1978; 31:337–340.
30. Lindon JC, Ferrige AG. Digitisation and data processing in Fourier transform NMR. *Prog NMR Spectrosc* 1980; 14:27–66.
31. Granot J. Resolution effects in spin-lattice relaxation time measurements. *J Magn Reson* 1982; 49:197–202.
32. Maudsley A, Wu Z, Meyerhoff DJ, Weiner MW. Automated processing for proton spectroscopic imaging using water reference deconvolution. *Magn Reson Med* 1994; 31:589–595.
33. Donoho DL. Nonlinear wavelet methods for recovery of signals, densities, and spectra from indirect and noisy data. In: Daubechies I, editor. *Different perspectives on wavelets, proceedings of symposia in applied mathematics*, vol. 47. Providence, RI: American Mathematical Society. 1993.
34. Gibbs A, Morris GA, Swanson AG, Cowburn D. Suppression of t_1 noise in 2D NMR spectroscopy by reference deconvolution. *J Magn Reson A* 1993; 101:351–356.
35. Horne TJ, Morris GA. Combined use of gradient-enhanced techniques and reference deconvolution for ultralow t_1 noise in 2D NMR spectroscopy. *J Magn Reson A* 1996; 123:246–252.
36. Barjat H, Morris GA, Smart S, Swanson AG, Williams SCR. High-resolution diffusion-ordered 2D spectroscopy (HR-DOSY)—a new tool for the analysis of complex mixtures. *J Magn Reson B* 1995; 108:170–172.
37. Barjat H, Morris GA, Swanson AG, Smart S, Williams SCR. Reference deconvolution using multiplet reference signals. *J Magn Reson A* 1995; 116:206–214.
38. Morris GA. Reference deconvolution in NMR. In: Rutledge DN, editor. *Signal treatment and signal analysis in NMR*. New York: Elsevier Science; 1996. p 346–361.
39. Morris GA, Barjat H, Horne TJ. Reference deconvolution methods. *J Progr Nucl Magn Reson Spectrosc* 1997; 31:197–257.
40. Ju J, Van QN, Mandelshtam VA, Shaka AJ. Reference deconvolution, phase correction and line listing of NMR spectra by the 1D filter diagonalization method. *J Magn Reson* 1998; 134:76–87.
41. Goez M, Heun R. Reference deconvolution in the frequency domain. *J Magn Reson* 1999; 136:69–75.
42. Koskinen MF, Metz K. The concentric loop-gap resonator—a compact, broadly tunable design for NMR applications. *J Magn Reson* 1992; 98:576–588.



Kenneth R. Metz received his Ph.D. in Physical Chemistry from the University of Arkansas at Fayetteville in 1982 for solid-state NMR studies of thallium compounds performed with James F. Hinton. Since 1987, he has occupied positions as Assistant Professor of Radiology at Harvard Medical School, Director of Basic Research at the Radiological Sciences Research Center of the New England Deaconess Hospital, and, most recently, as an independent consultant in magnetic

resonance. In addition to techniques and applications of NMR spectroscopy and imaging, Dr. Metz has research interests in cancer biochemistry, nanotechnology, and the history of chemistry. He is also an active collector of antique scientific instruments, early computers, and rare scientific books.



Michael M. Lam received his Ph.D. in Electrical and Computer Engineering at the University of Illinois at Urbana-Champaign in 1999 under the supervision of A. G. Webb. His research dealt with high resolution gradient-enhanced NMR microspectroscopy. He is currently enrolled in the M.D. program at UIUC and carrying out postdoctoral research in MRI monitoring of choroid plexus tumors in transgenic mice, and NMR microscopy of trabecular bone.



Andrew G. Webb received his Ph.D. in Medicinal Chemistry from the University of Cambridge in 1990, working for Laurie Hall on the development of new editing techniques for magnetic resonance imaging. He is an Associate Professor in the Department of Electrical and Computer Engineering, and the Beckman Institute for Advanced Science and Technology, at the University of Illinois at Urbana-Champaign. He heads a research team working on the development of solenoidal microcoils for high-resolution NMR spectroscopy of mass limited samples, the use of closed-loop feedback control in MRI monitored hyperthermia treatment of tumors, and functional MRI of cognitive processing involving attention.